# Optical properties and sulfate scattering efficiency of boundary layer aerosol at coastal Neumayer Station, Antarctica

**Rolf Weller[1] and Astrid Lampert[2]**

[1] Alfred Wegener Institute for Polar and Marine Research, Am Handelshafen 12, 27570 Bremerhaven, Germany
[2] Alfred Wegener Institute for Polar and Marine Research, Telegraphenberg A43, 14473 Potsdam, Germany

## Abstract

We measured optical properties and ionic composition of the aerosol at Neumayer Station from 2004 through 2006 by an integrating nephelometer and chemical analysis of daily aerosol samples, respectively. From this unique data set, we discussed the seasonality of optical parameters along with the chemical composition of the aerosol. Austral summer (November through March) was characterized by mean particle number concentrations of 472±260 $cm^{-3}$ compared to 168±160 $cm^{-3}$ during winter (April through October), mean scattering Ångström exponents of 1.5±0.6 compared to 1.2±0.5 during winter, and mean hemispheric backscattering ratios at 700 nm of 0.21±0.13 compared to 0.17±0.08 during winter. In contrast, light scattering coefficients ($\sigma_{sp}$) showed a broad maximum during winter (4.8±5.3 $Mm^{-1}$ for $\sigma_{sp}(550)$). The mean single scattering albedo was $0.99\pm^{0.01}_{0.02}$ at 550 nm. We further derived mass scattering and mass backscattering efficiencies for biogenic sulfate aerosol (BSA) at 450 nm, 550 nm, and 700 nm for relative humidities between 5% and 11%. At 550 nm the scattering efficiency for biogenic sulfate aerosol $\alpha^{s}_{BSA}(550)$ was 8.9±0.7 $m^2\ g^{-1}$ with a corresponding backscattering efficiency $\alpha^{bs}_{BSA}(550)$ of 1.0±0.08 $m^2\ g^{-1}$. From the seasonality of the aerosol composition, we inferred a dominant contribution of sulfate aerosol regarding radiative forcing in the lower troposphere from December through January, while the impact of sea salt aerosol prevailed for the rest of the year at Neumayer.

## 1. Introduction

Investigations of optical properties of atmospheric particles and their relation to physical condition (liquid, solid), size distribution, number density, and chemical composition are crucial to understand and assess radiative forcing entailed by aerosol (e.g. *Hatzianastassiou et al.,* [2004]; *McComiskey et al.,* [2008]). Concerning marine aerosol, such kind of measurements have been frequently conducted e.g. within the Aerosol Characterization Experiments ACE-1, ACE-2, ACE-3, and the Indian Ocean Experiment (INDOEX) [*Quinn et al.,* 1996, 1998, 2002, and 2004], but only rarely at high southern latitudes and Antarctica [*Bodhaine et al.,* 1986; *Bergin et al.,* 1998; *Quinn et al.,* 1996], which is the region least affected by civilization. Polar regions are characterized by high surface albedo and large solar zenith angles. Especially here, a detailed knowledge of the physico-chemical properties of the aerosol and their seasonality is required to assess the role of aerosol in radiative forcing [*Wuttke and Seckmeyer,* 2006]. Therefore one objective of our investigation was to document for the first time the seasonality of optical properties along with the chemical composition of boundary layer aerosol at coastal Antarctica. In addition, special emphasis was placed on determining mass scattering efficiencies of biogenic sulfate aerosol because marine phytoplankton is believed to be the major natural source for sulfuric acid particles and thus playing an important role in the Earth's energy balance [*Andreae and Crutzen,* 1997; *Gondwe et al.,* 2003]. Specific mass scattering efficiencies allow a direct and calculational easy conversion of aerosol mass to aerosol optical properties and are widely used in global circulation models assessing radiative forcing of a specific aerosol component [*Kinne et al.,* 2006]. Notational, for each aerosol component j the mass scattering efficiency $\alpha_j$ is defined by the partial derivative of the scattering coefficient $\sigma_j$ of that component $\partial\sigma_j/\partial m_j$ [*Anderson et al.,* 1994]. In practice, specific mass scattering efficiencies were essentially derived from light scattering measurements of natural aerosol mixtures in combination with chemical analyses of simultaneously sampled aerosol [*Quinn et al.,* 1996, 1998, 2002, and 2004; *Hand and Malm,* 2007]. Usually the obtained scattering efficiencies refer to dry aerosol (relative humidity, RH, typically below 40%) and have to be adjusted to the corresponding ambient RH for appliance in climate models [*McInnes et al.,* 1998]. Values for the sulfate scattering efficiency $\alpha_{sulfate}$ determined so far in the remote marine troposphere are within a wide range between 1.5 and 7.7 $m^2$ $g^{-1}$ [*Hegg et al.*, 1993; *Quinn et al.,* 1996, 1998, 2002, and 2004]. In all these previous assessments, the mass fraction of sulfate aerosol in the sub-micron range was typically well below 50% which may have hampered an unambiguous apportionment of the light scattering to sulfate aerosol [*Hegg et al.*, 1993]. At Neumayer, however, the aerosol budget during austral summer is frequently dominated by biogenic non sea salt sulfate (nss-$SO_4^{2-}$) and methane sulfonic acid (MSA) aerosol [*Minikin et al.,* 1998], allowing a more reliable apportionment of the light scattering to this portion of the aerosol.

## 2. Measurement Techniques and Methodology

Measurements were conducted at the Air Chemistry Observatory, Neumayer Station (70°39' S, 8°15'W, http://www.awi.de/en/go/air_chemistry_observatory) which participates in the Global Atmosphere Watch (GAW) programme. *König-Langlo et al.* [1998] described the climatology of this site and in *Weller et al.* [2002] aspects of contamination control of the sampling were reported. Concerning the representativeness of our measurements, one has to consider the characteristics of the boundary layer at this site. As typical for Antarctica, surface inversions are common. During winter the thickness of the surface inversion is up to about 2 km while from November to February inversions are rare and confined to heights less than 1 km [*König-Langlo et al.,* 1998]. Frequent stormy weather conditions usually destroy the stratification of the lower troposphere. The stable atmospheric boundary layer (SBL) at Neumayer has been investigated during two extended boundary layer experiments from 1983-1987 and 1994. Due to the stability of the free atmosphere above the boundary layer the typical height of the SBL, defined as the lowest altitude above ground where turbulent mixing ceased, ranged between 10 m and 50 m [*Handorf,* 1996].

From January 2004 through December 2006, aerosols were sampled for 24-hour time periods using a 2-stage PFA (polyfluoralkoxy-copolymer) filter holder system, including a teflon and a nylon (Nylasorb) filter (all 1 µm pore size). The optical aerosol properties were measured by means of a three wavelength integrating nephelometer (TSI, type 3563). A condensation particle counter (CPC, TSI, type 3022A) provided data on particle number concentrations (condensation particles, CP) for particles above a diameter of 10 nm. Black carbon (BC) concentrations were monitored by an aethalometer (Magee Scientific, type AE10). Aerosol measurements were further supported by an aerodynamic particle sizer (TSI, type APS 3321) providing data on aerosol size distributions from 0.542 µm to 10.4 µm aerodynamic diameter ($D_p$). All experiments installed in the Air Chemistry Observatory were under daily control and daily performance protocols are available. A ventilated stainless steel inlet stack (total height about 8 m above the snow surface) with a 50% aerodynamic cut-off diameter around 7-10 µm at wind velocities between 4-10 m $s^{-1}$ (determined with the APS 3321) supplied the experiments with ambient air.

The operation cycle of the nephelometer was set to 10 min average time and each hour a 10 min zero calibration with particle free air was automatically executed. The standard deviation of the zero calibration signal constituted the instrumental noise level. The detection limit was defined by a signal to noise ratio of two and ranged from 0.1 $Mm^{-1}$ to 0.3 $Mm^{-1}$ for the 10 min averages (1 $Mm^{-1}$ = $10^{-6}$ $m^{-1}$). Each year in January and after serious instrumental failure, we calibrated the nephelometer with particle free air as low span gas and $CO_2$ as high span gas. The performance of the operated nephelometer was estimated according to *Anderson et al.*

[1996]. Total scattering coefficients $\sigma_{sp}(\lambda)$ and hemispheric back scattering coefficients $\sigma_{bsp}(\lambda)$ were corrected for non-Lambertian illumination and truncation errors (so called angular nonidealities) according to *Anderson and Ogren* [1998] (Table 4a therein, "no-cut" case for back scattering and Table 4b therein, "no cut" case for total scattering). The impact of truncation error increases with increasing particle size especially for forward scattering. According to detailed investigations by *Anderson et al.,* [1996], the uncertainty for $\sigma_{sp}(\lambda)$ and $\sigma_{bsp}(\lambda)$ caused by nephelometer nonidealities is around 10% for sub-micron particles, increasing considerably (up to 20-50%) for total scatter in case of super-micron (coarse mode) aerosol. The used corrections for total scattering took into account the Ångström exponents from the uncorrected scattering coefficients, which were a rough estimate for the size distribution of the aerosol. This enabled a more adequate truncation correction [*Anderson and Ogren,* 1998]. Values below the detection limit (39 out of 6516 values) were excluded and not considered in determining averages as well as data points measured within potential impact of local contamination, indicated by elevated CP number concentrations (in summary less than 2% of the data). The scattering Ångström exponent å and the backscattering ratio b(λ) were calculated according to

$$å(450\text{-}700) = -\frac{\log(\sigma_{sp}(450)/\sigma_{sp}(700))}{\log(450/700)}$$

$$b(\lambda) = \sigma_{bsp}(\lambda)/\sigma_{sp}(\lambda)$$

where å(450-700) refers to the wavelength pair 450 nm and 700 nm.

Technical details about aerosol absorption measurements with an aethalometer can be found in *Hansen et al.* [1984] and *Hansen and McMurry* [1990]. Per se, the aethalometer measures (white) light absorption by aerosol sampled on a filter (in our case Pallflex, type T60A20). We used the calibration factor recommended by the manufacturer to first calculate the BC mass concentration (in ng/m$^3$). From this the aerosol absorption coefficient $\sigma_{ap}(550)$ can be calculated by using the specific cross section for BC aerosol suspended in air (10 m$^2$ g$^{-1}$) at a wavelength of 550 nm [*Clarke et al.,* 1986; *Bodhaine,* 1995]. The accuracy of absorption measurements by this method largely depends on the specific BC absorption, which may vary by a factor of 2 [*Liousse et al.*, 1993], and instrumental problems concerning light scattering effects on the used filter material [*Petzold and Schönlinner,* 2004]. As a consequence, the aerosol absorption coefficients $\sigma_{ap}$ presented here may have a relatively wide error margin of around ±100%.

For details concerning aerosol filter handling and analyses see *Piel et al.* [2006]. Generally, samples were analyzed by ion chromatography for methane sulfonate (MS), $Cl^-$, $Br^-$, $NO_3^-$, $SO_4^{2-}$, $Na^+$, $NH_4^+$, $K^+$, $Mg^{2+}$, and $Ca^{2+}$. In short, the combined uncertainty was approximately ±10% to ±15% for the main components MS, $Cl^-$, $NO_3^-$, $SO_4^{2-}$, $Na^+$, and between ±20% and ±30% for the minor species $NH_4^+$, $K^+$, $Mg^{2+}$, and $Ca^{2+}$. Non-sea salt sulfate (nss-$SO_4^{2-}$) mass concentrations were calculated by subtracting the mass concentration of the sea salt derived sulfate from the total $SO_4^{2-}$ mass concentration (unit: ng m$^{-3}$). We used $Na^+$ as sea salt reference species and the sulfate to sodium ratio in bulk sea water of $\alpha_{sulfate} = 0.252$ from November through February and $\alpha_{sulfate} = 0.07$ from March to October due to the potential impact of sea salt fractionation by frost flower formation [*Wagenbach et al.,* 1998] i.e.:

$$(\text{nss-}SO_4^{2-}) = (SO_4^{2-}) - \alpha_{sulfate} \times (Na^+)$$

We selected days where the ratio of the (nss-$SO_4^{2-}$+MS) mass concentration to the total mass concentration of all ions determined by IC, i.e. $R_{sulfate} = c(\text{nss-}SO_4^{2-}\text{+MS})/c(\text{ions})$, was higher than 0.75 for calculation of the scattering efficiency of biogenic sulfate aerosol. This was given on 62 days during polar summers within the observation period between January 2004 and end of December 2006. During these particular events the mean ± standard deviation (std) of the ambient temperature, ambient relative humidity (RH), and wind velocity were -5.4±4.6°C, 82±28%, and 6.8±4.0 m $s^{-1}$, respectively.

## 3. Results and Discussion

### 3.1. General Characterization of the Aerosol During the Observation Period

Time series of the measured scattering coefficients $\sigma_{sp}(550)$, hemispheric back scattering ratios b(700) = $\sigma_{bsp}(700)/\sigma_{sp}(700)$, scattering Ångström exponents å(450-700), and aerosol absorption $\sigma_{ap}(550)$ are presented in Figure 1. Mass concentrations of nss-$SO_4^{2-}$ and $Na^+$, as well as particle number concentrations are shown in Figure 2. Obviously all these parameters exhibited a more or less pronounced seasonality. Table 1 contrasts the mean summer (November through March) and winter (April through October) values. Figure 3 gives an overview on the ionic composition of the aerosol during summer and winter for the relevant measuring period. The results presented in Figures 2 and 3 are consistent with findings from our continuous long-term aerosol sampling programm established since 1983 [*Wagenbach et al.,* 1998; *Minikin et al.,* 1998]. While sea salt aerosol constituted the main aerosol component all over the year, austral summer at Neumayer was characterized by a sharp maximum of biogenic sulfur aerosol (i.e. MS and nss-$SO_4^{2-}$) between December and February, associated with more than an order of magnitude higher particle number concentrations compared to mid-winter (May through August).

On the whole the hourly averaged $\sigma_{sp}(\lambda)$ and $\sigma_{bsp}(\lambda)$ coefficients and their variability are comparable to those measured at remote Arctic sites like Pallas [*Aaltonen et al.,* 2006] and Barrow [*Delene and Ogren,* 2002] or the high-alpine site Jungfraujoch [*Collaud Coen et al.,* 2007], but nearly an order of magnitude higher compared to South Pole [*Bergin et al.,* 1998].

The low scattering coefficients at South Pole are mainly caused by significantly lower aerosol mass concentrations, especially for sea salt particles [*Arimoto et al., 2004*; *Harder et al.,* 2000].

The annual mean BC mass concentration was 1.3±2 ng $m^{-3}$ with a vague maximum around 2-3 ng $m^{-3}$ between September and November. Both, annual mean and seasonality of the atmospheric BC burden were comparable with analogous measurements performed at the Halley 5 station on the Brunt Ice Shelf [*Wolff and Cachier,* 1998]. The mean single scattering albedo, $\omega = \sigma_{sp}/(\sigma_{sp}+\sigma_{ap})$ of the aerosol was derived from $\sigma_{ap}$ and $\sigma_{sp}$ measurements (daily means in each case) at 550 nm. During the whole measuring period, >95% of the ω(550) values ranged between 1.00 and 0.97. Even considering the high error margin of $\sigma_{ap}$, (conservatively estimated to be ±100%), ω(550) values were never below 0.94 under clean air conditions, i.e. if no impact of local contamination indicated by enhanced CP number concentrations occurred.

## 3.2. Seasonality of Aerosol Optical Properties

Concerning optical properties, amplitudes and timing of the seasonal cycles were less distinct compared to nss-$SO_4^{2-}$ and CP. For b(700) a seasonality was virtually absent during 2004, while for b(450) as well as for b(550) no seasonal cycle was discernible throughout (not shown). Aerosol optical properties discussed here are primarily defined by complex refraction index, shape, and size distribution of the particle ensemble and not by its chemical composition. Nevertheless, these physical parameters of a particle are inherently linked with its chemical composition. We can assume that sulfate aerosol should be within the sub-micron size range, while sea salt particles are representative for the super-micron range, albeit with a considerable fraction in the accumulation mode [*Murphy et al.,* 1998]. According to Mie theory, å and b(λ) are completely defined by size distribution and complex refraction index and both, å and b(λ) are higher when the size distribution of the aerosol is dominated by sub-micron (i.e. accumulation-, Aitken-, and nucleation mode) particles [e.g. *Seinfeld and Pandis,* 1998, chapter 22]. Concordantly, observed å(450-700) and at least b(700) values were highest during summer at Neumayer and we found a significant correlation between scattering Ångström exponents and hemispheric back scattering ratios for all wavelengths, exemplarily shown for b(700) in Figure 4.

The back scattering ratios for 450 nm listed in Table 1 exceeded those of the longer wavelengths, which appeared inconsistent because for spherical particles, back scattering ratios should essentially decrease with increasing $D_p/\lambda$ ratio due to more pronounced forward scattering. We believe that this discrepancy and the lack of a seasonality for b(450) and b(550) were artefacts largely caused by the vastly differing truncation correction factors for total scatter (but not for backscatter) at these wavelengths for sub-micron and super-micron aerosol [*Anderson and Ogren,* 1998]. In our case, truncation corrections seemed to underestimate total scatter, especially during winter. The applicability of the mentioned correction factors is restricted to spherical particles and refers to a lognormal size distribution with a geometric std of 1.8 [*Anderson and Ogren,* 1998]. Hence, especially during winter when the dominance of sea salt aerosol caused a shift in the size distribution to higher $D_p$, overall correction factors are not adequate. In addition sea salt particles should be non-spherical inside the nephelometer due to low RH. In this case, a separate determination of the back scattering ratio for sub-micron and super-micron particles would be reasonable [*Anderson and Ogren,* 1998], which was not possible with our experimental set-up.

### 3.3. Aerosol properties during $R_{sulfate} > 0.75$

Table 2 presents a summary of the chemical composition of the aerosol during $R_{sulfate} >$ 0.75. Due to the lack of size-segregated aerosol chemistry investigations at Neumayer, we rely on relevant measurements from the Finnish station Aboa [*Teinilä et al.,* 2000], where the summertime aerosol showed ionic concentrations comparable to Neumayer. Those studies revealed a comparable mass size distribution for the aerosol compounds nss-$SO_4^{2-}$, MS and $NH_4^+$ with a dominant mode in the accumulation size range at about 0.3 µm (RH between 47% and 75%), indicating that these ions were internally mixed. Nitrate was found nearly exclusively in the super micron size range, most probably associated with sea salt particles [*Teinilä et al.,* 2000]. Indeed, results from combined FTIR spectrometer and sun photometer measurements at Neumayer in January/February 2000 supported the prevalence of an acidic internal $H_2O$(ice)-$(NH_4)_2SO_4$-$H_2SO_4$ aerosol mixture [*Rathke et al.,* 2002]. Consequently, we are confident that the aerosol fraction determining the light scattering was an internal mixture of $H_2O$-$(NH_4)HSO_4$-$H_2SO_4$-MSA in the sub-micron (accumulation) mode with a negligible portion of sub-micron sea salt aerosol.

The main advantage determining optical properties at low RH (typically below 40%) is that variations can largely be attributed to changes of concentration and/or nature of aerosol particles and not to variations in relative humidity. Unfortunately, sulfuric acid particles show hygroscopic growth under virtually all atmospheric humidity conditions [*Tang and Munkelwitz*, 1994]. In our case, the RH was generally between 5% and 11% in the nephelometers' measuring volume. According to the Aerosol Inorganic Model (AIM, (http://www.hpc1.uea.ac.uk/~e770/aim.html, [*Clegg et al.* 1998]) and neglecting the minor sea salt portion, the mean aerosol composition inside the nephelometer under these conditions should be around 60%-75% $H_2SO_4$, 25%-40% $H_2O$ and 2.6% $NH_3$. As input parameters we used $H_2SO_4$ = 2.85 nmol, $NH_3$ = 0.6 nmol, $H^+$ = 5.1 nmol, p($H_2O$) = 380 Pa at 300 K and p($H_2O$) = 396 Pa at 313 K (MSA could not be considered by the model and was treated as sulfuric acid).

Concerning the optical aerosol properties under $R_{sulfate}$ > 0.75, we derived scattering Ångström exponents å(450-700) = 2.3±0.3 (mean±std) and mean backscattering ratios above 0.2 for all wavelengths (Table 3). These findings supported again the dominance of sub-micron aerosol in light scattering during $R_{sulfate}$ >0.75.

**3.4. Scattering Efficiency of Biogenic Sulfate Aerosol (BSA)**

Due to the fact that we have to suppose BSA being an internal mixture of $H_2SO_4$-MSA-$H_2O$ (with a minor $NH_3$ contingent) at Neumayer, an apportionment of light extinction to the individual components is not legitimated. For internal aerosol mixtures specific scattering efficiencies are not additive but dependent on the particular contingent of each component in the mixture which is usually impossible to disentangle [*White,* 1986]. Nevertheless we referred to nss-$SO_4^{2-}$ as a indicator ion for biogenic sulfate aerosol. In order to derive the sulfate scattering efficiency we correlated the total scattering coefficients $\sigma_{sp}(\lambda)$ and backscattering coefficients $\sigma_{bsp}(\lambda)$ with the biogenic sulfate aerosol mass concentration c(nss-$SO_4^{2-}$) during $R_{sulfate}$ >0.75 (Figures 5 and 6). The parameters of reduced major axis (RMA) regression fits are summarized in Tables 3 and 4. Our results for the scattering efficiency of BSA at 550 nm ($\alpha^s_{BSA}(550)$ = 8.9±0.7 $m^2\ g^{-1}$) appeared somewhat high compared to $\alpha^s_{sulfate}(550)$ values obtained so far in the remote marine troposphere. *Hegg et al.* [1993] determined $\alpha^s_{sulfate}(550)$ to be 2.84±0.14 $m^2\ g^{-1}$ in the northeast Atlantic, while values between 1.5 and 7.7 $m^2\ g^{-1}$ were found in the MBL of the Pacific and Indian Ocean [*Quinn et al.,* 1996, 1998, 2002, and 2004]. The latter authors determined backscattering efficiency $\alpha^{bs}_{sulfate}(550)$ to be between 0.40 and 0.48 $m^2\ g^{-1}$ which are roughly a factor of two lower compared to our result (Table 4). In these previous investigations sulfate was most commonly a minor constituent of the total submicron aerosol mass concentration and the results applied to higher RH between 20% and 45% inside the instrument and thus higher water content of the aerosol in the measuring volume, while our scattering coefficients refer to an internal mixture of $H_2SO_4$-MSA-$H_2O$ (with a minor $NH_3$ but high MSA contingent) at RH between 5% and 11% inside the nephelometer.

Alternatively we correlated our measured light scattering coefficients with the sum of the MS and nss-$SO_4^{2-}$ mass concentrations c(nss-$SO_4^{2-}$+MS) explicitly considering MS, but implicating the same scattering efficiency for nss-$SO_4^{2-}$ and MS. This approach resulted in $\alpha^{s}_{sulfate+MS}(550) = 5.1\pm0.5$ m$^2$ g$^{-1}$ (but with a poorer regression coefficient $r^2 = 0.66$), in good agreement with the commonly adopted value of $\alpha^{s}_{sulfate}$ (550) = 5±2 m$^2$ g$^{-1}$ [*Charlson et al.,* 1992]. Note that the hitherto derived $\alpha^{s}_{sulfate}(550)$ values mentioned above refer to marine sulfate at lower latitudes where the MS portion is typically much lower compared to polar regions [*Gondwe et al.*, 2004]. The high $\alpha^{s}_{BSA}$ values derived here refer to nss-$SO_4^{2-}$ mass concentrations implicitly including the high MS contingent of the internally mixed BSA aerosol.

Statistically, (75-77)% of the variance of $\sigma_{sp}(\lambda)$ and (81-86)% of the variance of $\sigma_{bsp}(\lambda)$ were finally explained by variations of c(nss-$SO_4^{2-}$) (Tables 3 and 4). Generally all factors determining size distribution and refraction index of the aerosol have an impact on the scattering coefficients $\sigma_{sp,bsp}(\lambda)$. Consequently, a significant part of the observed variance was probably caused by a combination of: (i) the presence of an aerosol fraction in the sub-micron range with different scattering efficiency, most probably sea salt aerosol, (ii) a mutable size distribution (e.g. caused by varying relative humidity), (iii) changing refractive index. The impact of these factors on $\sigma_{sp,bsp}(\lambda)$ could be antipodal (e.g. higher humidity should result in a larger mean modal diameter but lower refractive index) and could not be assessed on the basis of the available data.

### 3.5. Implications for light scattering by sulfate and sea salt aerosol over Antarctica

In the following we will compare the importance of biogenic sulfate aerosol in terms of radiative forcing with sea salt aerosol at Neumayer. From Figure 3 it is obvious that the total aerosol budget at Neumayer is dominated by sea salt particles. Especially during winter, sea salt aerosol constituted typically about 90% of the total aerosol mass. Here, low Ångström exponents and high aerosol mass concentration at low particle number densities (Figures 1 and 2) indicated the presence of super-micron sea salt particles. Due to the fact that we could not differentiate between sub- and super-micron mode of the aerosol in our measurements, a corresponding correlation of the scattering coefficients versus c(sea salt) resulted in a poor regression ($r^2 < 0.25$) even when more than 90% of the aerosol mass consisted of sea salt particles. Notwithstanding, from the individual $\sigma_s(550)$/c(sea salt) ratios under the condition that c(sea salt)/c(ions) was > 0.9 (n = 178 data points) we calculated an overall mean scattering efficiency for sea salt particles of $\alpha^s_{ss}(550) = 5\pm3$ m$^2$ g$^{-1}$. For comparison, *Quinn et al.* [1996] determined for high latitude Pacific regions $\alpha^s_{ss}(550) = 5.5\pm0.22$ m$^2$ g$^{-1}$ for sub-micron and 0.68±0.08 m$^2$ g$^{-1}$ for super-micron sea salt aerosol, respectively. Overall, the scattering efficiency for sea salt aerosol appeared roughly a factor of 1.7 lower compared to biogenic sulfate aerosol. Nevertheless, except the period from December through January, scattering of solar radiation at Neumayer was dominated by sea salt particles. In continental Antarctica, on the other hand, the role of biogenic sulfate aerosol in terms of light scattering seems to be much more pronounced. Recent year-round aerosol measurements at Kohnen Station (75°S, 0°E) [*Weller and Wagenbach,* 2007] revealed an order of magnitude lower sea salt aerosol load accompanied by roughly comparable nss-$SO_4^{2-}$ mass concentrations (Figure 7). Under these conditions, scattering of clear-sky solar radiation in the lower atmosphere can primarily be ascribed to biogenic sulfate aerosols.

## 4. Conclusion

Aerosol optical properties at Neumayer are largely characterized by sea salt and biogenic sulfate particles, the latter showing a distinct seasonality with a strong summer maximum which may be succinctly termed as biogenic haze (although the term haze is exaggerated considering that $\sigma_{sp}$ never exceeded 10 $Mm^{-1}$ in such cases). In particular from December through January, optical properties of boundary layer aerosol were most frequently determined by sulfate aerosol, while for the rest of the year the impact of sea salt aerosol dominated. There is a large variability in sulfate and sea salt scattering efficiencies measured so far in the remote marine troposphere, caused by the natural variability in aerosol properties. Accordingly, an unique (i.e. global) sulfate mass scattering efficiency can not be expected. Nevertheless the presented scattering efficiencies should be especially reliable for the marine atmosphere at high southern latitudes, where the budget of sulfate aerosol is dominated by biogenic sources with a relatively high amount of MS. The obtained high mass scattering efficiencies and back scattering ratios for biogenic sulfate aerosol in combination with high summertime mass concentrations (when incident solar radiation is maximal) emphasize the significance of dimethyl sulfide (DMS) derived aerosol on the tropospheric radiative balance over the Southern Ocean which has recently been demonstrated by remote sensing data [*Gabric et al.,* 2005; *Meskhidze and Nenes,* 2006]. For the Pacific from 55°N to 70°S, however, sea salt seems to dominate the aerosol mass in the marine boundary layer, even in the submicron size range and should be the main contributor to light scattering by aerosol [*Quinn and Coffman,* 1999].

While over the ice free Southern Ocean a net cooling effect of the aerosol layer can be expected due to low surface albedo [e.g. *Hatzianastassiou et al.,* 2004], the situation is more subtle over regions with high surface albedo. Daily mean spectral albedo data for a flat snow surface at Neumayer showed a broad maximum of 0.98 at wavelengths between 420 nm and 500 nm [*Wuttke et al.,* 2006], suggesting here a delicate dependence of the radiative balance on the single scattering albedo ω. Clearly, assessing the impact of the aerosol considered here on clear-sky radiative balance for ice covered Antarctica needs comprehensive model calculations. In addition, due to the lack of corresponding data, our results refer to surface observations primarily representative for the stable boundary layer. They discount the vertical structure of the aerosol layer and the changing physico-chemical properties of particles with altitude, emphasizing the need for corresponding field measurements.

**Acknowledgements.** The authors would like to thank Gert König-Langlo for providing the meteorological data used in this contribution. We also acknowledge the valuable comments of three anonymous reviewers that helped to improve the paper. Special thanks go to Renate Treffeisen and Christoph Ritter for fruitful discussions and the technicians and scientists of the Neumayer overwintering crews of the years 2004 through 2006. This is AWI publication no. 17179. Data are available from Pangaea (doi:10.1594/PANGAEA.695432).

## References

Aaltonen, V., H. Lihavainen, V.-M. Kerminen, M. Komppula, J. Hatakka, K. Eneroth, M. Kulmala, and Y. Viisanen (2006), Measurements of optical properties of atmospheric aerosol in Northern Finland, *Atmos. Chem. Phys., 6*, 1155-1164.

Andreae, M.O., and P.J. Crutzen (1997), Atmospheric aerosols: Biogeochemical sources and role in atmospheric chemistry, *Science, 276*, 1052-1058.

Anderson, T.L., R.J. Charlson, W.H. White, and P.H. McMurry (1994), Comment on “Light scattering and cloud condensation nucleus activity of sulfate aerosol measured over the Northeast Atlantic Ocean” by D.A. Hegg et al., *J. Geophys. Res., 99*(D12), 25,947-25,949.

Anderson, T.L. et al. (1996), Performance characteristics of a high-sensitivity, three-wavelength, total scatter/backscatter nephelometer, *Journal of Atmospheric and Oceanic Technology, 13,* 967-986.

Anderson, T.L., and J.A. Ogren (1998), Determining aerosol radiative properties using the TSI 3563 integrating nephelometer, *Aerosol Sci. Technol., 29,* 57-69.

Arimoto, R., A. Hogan, P. Grube, D. Davis, J. Webb, C. Schloesslin, S. Sage, F. Raccah (2004), Major ions and radionuclides in aerosol particles from the South Pole during ISCAT-2000, *Atmos. Environ., 3*8, 5473-5484.

Bergin, M.H., E.A. Meyerson, J.E. Dibb, and P.A. Mayewski (1998), Relationship between continuous aerosol measurements and firn core chemistry over a 10-year period at South Pole, *Geophys. Res. Lett., 25*(8), 1189-1192.

Bodhaine, B.A. (1995), Aerosol absorption measurements at Barrow, Mauna Loa and the south pole, *J. Geophys. Res., 100*(D5), 8967-8975.

Bodhaine, B.A., J.J. Deluisi, J.M. Harris, P. Houmere, and S. Bauman (1986), Aerosol measurements at South Pole, *Tellus, 38*B, 223-235.

Charlson, R.J., S.E. Schwartz, J.M. Hales, R.D. Cess, J.A. Coakley Jr., J.E. Hansen, and D.J. Hofmann (1992), Climate forcing by anthropogenic aerosols, *Science, 255,* 423-430.

Clarke, A.D., K.J. Noone, J. Heintzenberg, S.G. Warren, and D.S. Covert (1986), Aerosol light absorption measurement techniques: analysis and intercomparisons, *Atmos. Environ. 21* (6), 1455-1465.

Clegg S. L., P. Brimblecombe, and S.A. Wexler (1998), A thermodynamic model of the system $H^+$ - $NH_4^+$ - $SO_4^{2-}$ - $NO_3^-$ - $H_2O$ at tropospheric temperatures. *J. Phys. Chem. A 102*, 2137-2154.

Collaud Coen, M., E. Weingartner, S. Nyeki, J. Cozic, S. Henning, B. Verheggen, R. Gehrig, and U. Baltensperger (2007), Long-term trend analysis of aerosol variables at the high-alpine site Jungfraujoch, *J. Geophys. Res., 112,* D13213, doi:10.1029/2006JD007995.

Delene, D.J. and J.A. Ogren (2002), Variability of Aerosol Optical Properties at Four North American Surface Monitoring Sites, *J. Atmos. Sci., 59,* 1135-1150.

Gabric, A.J., J.M. Shephard, J.M. Knight, G. Jones, and A.J. Trevena (2005), Correlations between the satellite-derived seasonal cycles of phytoplankton biomass and aerosol optical depth in the Southern Ocean: Evidence for the influence of sea ice, *Global Biogeochem. Cycles, 19*, GB4018, doi:10.1029/2005GB002546.

Gondwe, M., M. Krol, W. Gieskes, W. Klaassen, and H. de Baar (2003), The contribution of ocean-leaving DMS to the global atmospheric burdens of DMS, MSA, $SO_2$, and NSS $SO_4^=$, *Global Biogeochem. Cycles, 17*(2), 1056, doi:10.1029/2002GB001937.

Gondwe, M., M. Krol, W. Klaassen, W. Gieskes, and H. de Baar (2004), Comparison of modelled versus measured MSA:NSS $SO_4^=$ ratios: A global analysis, *Global Biogeochem. Cycles, 18,* GB2006, doi:10.1029/2003GB002144.

Hand, J.L. and W.C. Malm (2007), Review of aerosol mass scattering efficiencies from ground-based measurements since 1990, *J. Geophys. Res., 112,* D16203, doi:10.1029/2007JD008484.

Handorf, D. (1996), Zur Parametrisierung der stabilen atmosphärischen Grenzschicht über einem antarktischen Schelfeis, in *Reports on Polar and Marine Research, 204,* edited by F. Riemann, Alfred-Wegener-Inst. for Polar and Marine Res., Bremerhaven.

Hansen, A.D.A., H. Rosen, and T. Novakov (1984), The aethalometer–An instrument for the real-time measurement of optical absorption by aerosol particles, *Sci. Total Environ., 36*, 191-196.

Hansen, A.D.A. and P.H. McMurry (1990), An intercomparison of measurements of aerosol elemental carbon during the 1986 carbonaceous species method comparison study, *Journal of the Air & Waste management Association, 40,* 894-895, 1990.

Harder, S., S.G. Warren, and R.J. Charlson (2000), Sulfate in air and snow at the South Pole: Implications for transport and deposition at sites with low snow accumulation, *J. Geophys. Res., 105*(D18), 22,825-22,832.

Hatzianastassiou, N., B. Katsoulis, and I. Vardavas (2004), Global distribution of aerosol direct radiative forcing in the ultraviolet and visible arising under clear skies, *Tellus, 56B*, 51-71.

Hegg, D.A, R.J. Ferek, and P.V. Hobbs (1993), Light scattering and cloud condensation nucleus activity of sulfate aerosol measured over the Northeast Atlantic Ocean, *J. Geophys. Res., 98*(D8), 14,887-14,894.

Kinne, S. et al. (2006), An AeroCom initial assessment – optical properties in aerosol component modules of global models, *Atmos. Chem. Phys., 6*, 1815-1834.

König-Langlo, G., J.C. King, P. Pettré (1998), Climatology of the three coastal Antarctic stations Dumont d'Urville, Neumayer, and Halley, *J. Geophys. Res., 103*(D9), 10,935-10,946.

Liousse, C., H. Cachier, and S.G. Jennings (1993), Optical and thermal measurements of black carbon aerosol content in different environments: Variation of the specific attenuation cross-section sigma (σ), *Atmos. Environ., 27A*, 1203-1211.

McComiskey, A., S.E. Schwartz, B. Schmid, H. Guan, E.R. Lewis, P. Ricchiazzi, and J.A. Ogren (2008), Direct aerosol forcing: Calculation from observables and sensitivities to inputs, *J. Geophys. Res., 113,* D09202, doi:10.1029/2007/JD009170.

McInnes, L., M. Bergin, J. Ogren, and S. Schwartz (1998), Apportionment of light scattering and hygroscopic growth to aerosol composition, *Geophys. Res. Lett., 25*(4), 513-516.

Meskhidze, N. and A. Nenes (2006), Phytoplankton and Cloudiness in the Southern Ocean, *Science, 314,* 1419-1423.

Minikin, A., M. Legrand, J. Hall, D. Wagenbach, C. Kleefeld, E. Wolff, E.C. Pasteur, and F. Ducroz (1998), Sulfur-containing species (sulfate and methanesulfonate) in coastal Antarctic aerosol and precipitation, *J. Geophys. Res.*, *103*(D9), 10,975-10,990.

Murphy, D.M., J.R. Anderson, P.K. Quinn, L.M. McInnes, F.J. Brechtel, S.M. Kreidenweis, A.M. Middlebrook, M. Pósfai, D.S. Thomson, and P.R. Busek (1998), Influence of sea-salt on aerosol radiative properties in the Southern Ocean marine boundary layer, *Nature, 392*(5), 62-65.

Petzold, A. and Schönlinner, M. (2004), Multi-angle absorption photometry – a new method fort the measurement of aerosol light absorption and atmospheric black carbon, *Aerosol Science 35,* 421-441.

Piel, C., R. Weller, M. Huke, and D. Wagenbach (2006), Atmospheric methane sulfonate and non-sea salt sulphate records at the EPICA deep-drilling site in Dronning Maud Land, Antarctica, *J. Geophys. Res.*, 111, D03304, doi:10.1029/2005JD006213.

Quinn, P.K., V.N. Kapustin, T.S. Bates, and D.S. Covert (1996), Chemical and optical properties of marine boundary layer aerosol particles of the mid-Pacific in relation to sources and meteorological transport, *J. Geophys. Res., 101*(D3), 6931-6951.

Quinn, P.K. and D.J. Coffman (1999), Comment on “Contribution of different aerosol species to the global aerosol extinction optical thickness: Estimates from model results” by Tegen et al., *J. Geophys. Res., 104*(D4), 4241-4248.

Quinn, P.K., D.J. Coffman, V.N. Kapustin, T.S. Bates, and D.S. Covert (1998), Aerosol optical properties in the marine boundary layer during the First Aerosol Characterization Experiment (ACE 1) and the underlying chemical and physical aerosol properties, *J. Geophys. Res., 103*(D13), 16,547-16,563.

Quinn, P.K., D.J. Coffman, T.S. Bates, T.L. Miller, J.E. Johnson, E.J. Welton, C. Neusüss, M. Miller, and P.Sheridan (2002), Aerosol optical properties during INDOEX 1999: Means, variabilities, and controlling factors, *J. Geophys. Res., 107*(D19), 8020, doi:10.1029/2000JD000037.

Quinn, P.K. et al. (2004), Aerosol optical properties measured on board the *Ronald H. Brown* during ACE-Asia as a function of aerosol chemical composition and source region, *J. Geophys. Res., 109*, D19S01, doi:10.1029/2003JD004010.

Rathke, C., J. Notholt, J. Fischer, and A. Herber (2002), Properties of coastal Antarctic aerosol from combined FTIR spectrometer and sun photometer measurements, *Geophys. Res. Lett., 29*(23), 2131, doi:10.1029/2002GL015395.

Seinfeld, J.H., and S.N. Pandis (1998), *Atmospheric Chemistry and Physics, From Air Pollution to Climate Change*, John Wiley, Hoboken, N.J.

Tang, I.N., and H.R. Munkelwitz (1994), Water activities, densities, and refractive indices of aqueous sulfates and sodium nitrate droplets of atmospheric importance, *J. Geophys. Res., 99*(D9), 18,801-18,808.

Teinilä, K., V.-M. Kerminen, and R. Hillamo (2000), A study of size-segregated aerosol chemistry in the Antarctic atmosphere, *J. Geophys. Res., 105*(D3), 3893-3904.

Wagenbach, D., F. Ducroz, R. Mulvaney, L. Keck, A. Minikin, M. Legrand, J.S. Hall, and E.W. Wolff (1998), Sea salt aerosol in coastal Antarctic regions, *J. Geophys. Res.*, *103*(D9), 10,961-10,974.

Weller, R., A.E. Jones, A. Wille, H.-W. Jacobi, H.P. McIntyre, W.T. Sturges, M. Huke, D. Wagenbach (2002), Seasonality of reactive nitrogen oxides ($NO_y$) at Neumayer Station, Antarctica, *Journal of Geophysical Research, 107*(D23), 4673,doi:10.1029/2002JD002495.

Weller, R. and D. Wagenbach (2007), Year-round chemical aerosol records in continental Antarctica obtained by automatic samplings, *Tellus, 59B*, 755-765.

White, W.H. (1986), On the theoretical and empirical basis for apportioning extinction by aerosols: A critical review, *Atmos. Environ., 20*(9), 1659-1672.

Wolff, E.W. and H. Cachier (1998), Concentrations and seasonal cycle of black carbon in aerosol at a coastal Antarctic station, *J. Geophys. Res., 103*(D9), 11,033-11,041.

Wuttke, S., and G. Seckmeyer (2006), Spectral radiance and sky luminance in Antarctica: a case study, *Theor. Appl. Climatol.,85,* 131-148, doi:10.1007/s00704-005-0188-2.

Wuttke, S., G. Seckmeyer, and G. König-Langlo (2006), Measurements of spectral snow albedo at Neumayer, Antarctica, *Annales Geophysicae, 24,* 7-21.

**Table 1.** Seasonality of optical and chemical properties of tropospheric aerosol at Neumayer measured from 2004 through 2006; summer is from November through March, winter from April through October, c(seasalt) = c($Na^{+}$+$Mg^{2+}$+$Cl^{-}$+$Br^{-}$+ss-$SO_4^{2-}$).

| parameter | summer (mean±std) | winter (mean±std) |
|---|---|---|
| nss-$SO_4^{2-}$ | 256±141 ng $m^{-3}$ | 68±44 ng $m^{-3}$ |
| MS | 102±120 ng $m^{-3}$ | 9±18 ng $m^{-3}$ |
| m(sea salt) | 597±830 ng $m^{-3}$ | 844±1100 ng $m^{-3}$ |
| $\sigma_{sp}$(450) | 4.2±3.3 $Mm^{-1}$ | 6.1±7.4 $Mm^{-1}$ |
| $\sigma_{sp}$(550) | 3.2±2.9 $Mm^{-1}$ | 4.8±5.3 $Mm^{-1}$ |
| $\sigma_{sp}$(700) | 2.4±2.5 $Mm^{-1}$ | 4.1±5.5 $Mm^{-1}$ |
| b(450)* | 0.21±0.07 | 0.2±0.09 |
| b(550)* | 0.19±0.05 | 0.17±0.07 |
| b(700) | 0.21±0.13 | 0.17±0.08 |
| å(450-700) | 1.5±0.6 | 1.2±0.5 |
| $\sigma_{ap}$(550) | 0.015±0.014 $Mm^{-1}$ | 0.017±0.018 $Mm^{-1}$ |
| particle concentration | 472±261 $cm^{-3}$ | 168±162 $cm^{-3}$ |

* values potentially biased by inadequate truncation correction.

**Table 2.** Summary of the aerosol composition during the relevant days with c(nss-$SO_4^{2-}$+MS)/c(ions) ratios above 0.75. The $H^+$ concentration was calculated from the measured ion balance assuming that the difference between the anion and the cation equivalents corresponds roughly to the $H^+$ equivalents. The $H^+$ fraction is given in ion equivalent percent (eq%); c(seasalt) = c($Na^+$+$Mg^{2+}$+$Cl^-$+$Br^-$+ss-$SO_4^{2-}$).

| Component | value (mean±std) | fraction (mean±std) |
|---|---|---|
| nss-$SO_4^{2-}$ | 351±160 ng $m^{-3}$ | (59.0±8.7)% |
| MS | 147±110 ng $m^{-3}$ | (21.8±7.8)% |
| $Cl^-$ | 44.1±29 ng $m^{-3}$ | (7.4±3.1)% |
| $NO_3^-$ | 29.1±15 ng $m^{-3}$ | (5.1±2.4)% |
| $Na^+$ | 19±20 ng $m^{-3}$ | (3.2±2.8)% |
| $NH_4^+$ [ng $m^{-3}$] | 17.6±15 ng $m^{-3}$ | (2.9±2.3)% |
| m(ions) | 613±306 ng $m^{-3}$ | 100% |
| m(nss-$SO_4^{2-}$+MS) | 515±267 ng $m^{-3}$ | (83.6±5.1)% |
| m(sea salt) | 68.5±52 ng $m^{-3}$ | (11.3±5.5) |
| $H^+$ | 8.1±4.2 ng $m^{-3}$ | (80.3±12) eq% |
| particle concentration | 498±230 $cm^{-3}$ | - |
| black carbon | 1.4±2.1 ng $m^{-3}$ | (0.4±0.6)% |

**Table 3.** Scattering efficiency of nss-$SO_4^{2-}$ aerosol $\alpha^{s}_{BSA}(\lambda)$ derived from RMA regression of $\sigma_{sp}(\lambda)$ vs. c(nss-$SO_4^{2-}$) shown in Figure 1. Y-axis intercept = $\varepsilon^{s}$, regression coefficient = $r^2$, and backscattering ratio $b(\lambda) = \sigma_{bsp}(\lambda)/\sigma_{sp}(\lambda)$.

| Wavelength λ [nm] | $\alpha^{s}_{BSA}(\lambda)$ [$m^2\ g^{-1}$] | $\varepsilon^{s}$ [$m^2\ g^{-1}$] | $r^2$ | b(λ) |
|---|---|---|---|---|
| 450 | 13.9±1.1 | -1.1±1.0 | 0.77 | 0.202±0.074 |
| 550 | 8.9±0.7 | -0.78±0.66 | 0.77 | 0.201±0.052 |
| 700 | 5.2±0.4 | -0.47±0.04 | 0.75 | 0.244±0.074 |

**Table 4.** Back-scattering efficiency of biogenic sulfate aerosol $\alpha^{bs}_{BSA}(\lambda)$ derived from RMA regression of $\sigma_{bsp}(\lambda)$ vs. c(nss-$SO_4^{2-}$) shown in Figure 2 (abbreviations see Table 3).

| Wavelength λ [nm] | $\alpha^{bs}_{BSA}(\lambda)$ [$m^2\ g^{-1}$] | $\varepsilon^{bs}$ [$m^2\ g^{-1}$] | $r^2$ |
|---|---|---|---|
| 450 | 1.2±0.09 | 0.18±0.08 | 0.81 |
| 550 | 1.0±0.08 | 0.034±0.06 | 0.85 |
| 700 | 0.83±0.05 | 0.004±0.05 | 0.86 |

**FIGURES**

**Figure 1:** Time series of (a) scattering coefficients $\sigma_{sp}(550)$, (b) hemispheric back-scattering ratios b(700), scattering Ångström exponents å(450-700), and (d) absorption coefficients $\sigma_{ap}(550)$. Daily means are displayed in light grey and 31-days running means by the bold line in dark grey.

**Figure 2:** Time series of (a) nss-$SO_4^{2-}$ and (b) $Na^+$ mass concentrations and (c) condensation particle (CP) number concentrations. Daily means are displayed in light grey and 31-days running means by the bold line in dark grey.

**Figure 3:** Mean ionic composition of the aerosol at Neumayer for (a) summer and (b) winter during the total measuring period (Jan. 2004 to Dec. 2006).

**Figure 4:** Back scattering ratios b(700) versus scattering Ångström exponent å(450-700) for the total measuring period (Jan. 2004 through Dec. 2006); circles: summer data, dots: winter data.

**Figure 5:** Dependence of scattering coefficients $\sigma_{sp}(\lambda)$ on nss-$SO_4^{2-}$ mass concentrations during days with c(nss-$SO_4^{2-}$+MS)/c(ions) >0.75. The lines represent RMA regression fits to the measuring points (see Table 3).

**Figure 6:** Dependence of hemispheric backscattering coefficients $\sigma_{bsp}(\lambda)$ on nss-$SO_4^{2-}$ mass concentrations during days with c(nss-$SO_4^{2-}$+MS)/c(ions) >0.75. The lines represent RMA regression fits to the measuring points (see Table 4).

**Figure 7:** Monthly mean values of nss-$SO_4^{2-}$ and sea salt mass concentrations measured (a) at Neumayer, and (b) at Kohnen. All monthly mean values from Neumayer comprise measurements between January 2004 and December 2006, while the Kohnen data were obtained between January 2003 and December 2005 [*Weller and Wagenbach,* 2007].

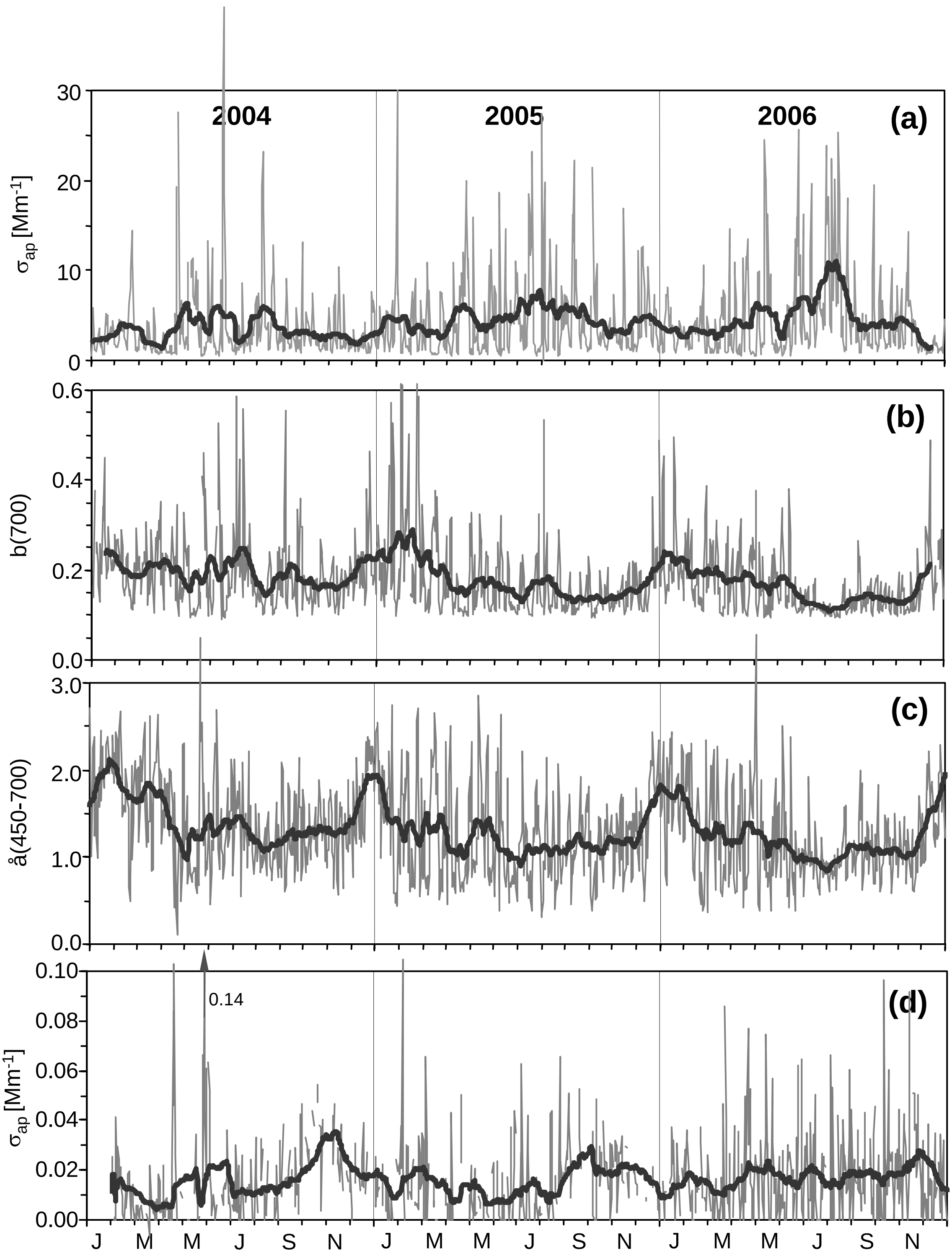


**Figure 1:** Time series of (a) scattering coefficients $\sigma_s(550)$. (b) hemispheric back-scattering ratios b(700), (c) scattering Ångström exponents å(450-700), and (d) absorption coefficients $\sigma_{ap}(550)$. Daily means are displayed in light grey and 31-days running means by the bold line in dark grey.

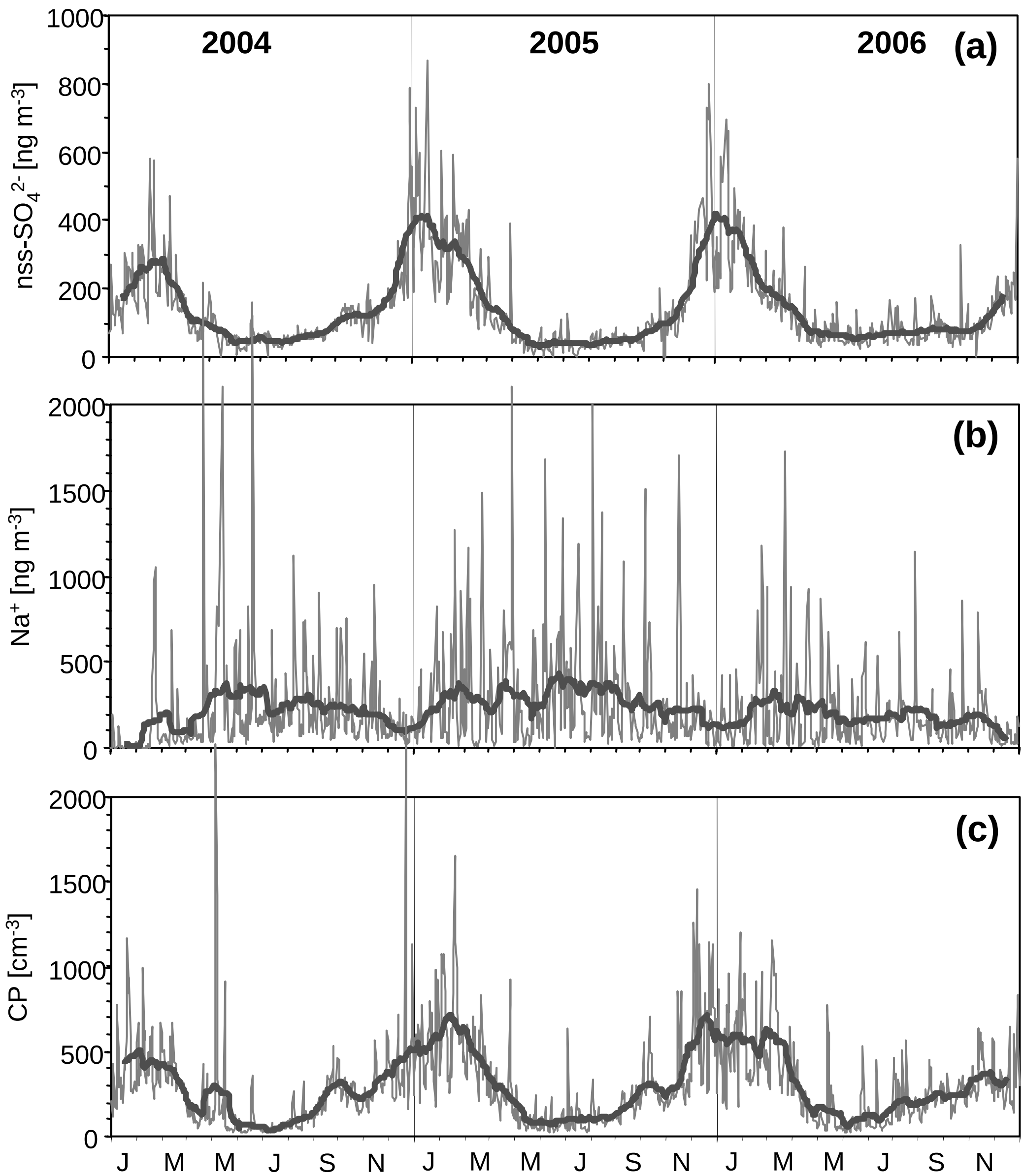


**Figure 2:** Time series of (a) nss-$SO_4^{2-}$ and (b) $Na^+$ mass concentrations and (c) condensation particle (CP) number concentrations. Daily means are displayed in light grey and 31-days running means by the bold line in dark grey.

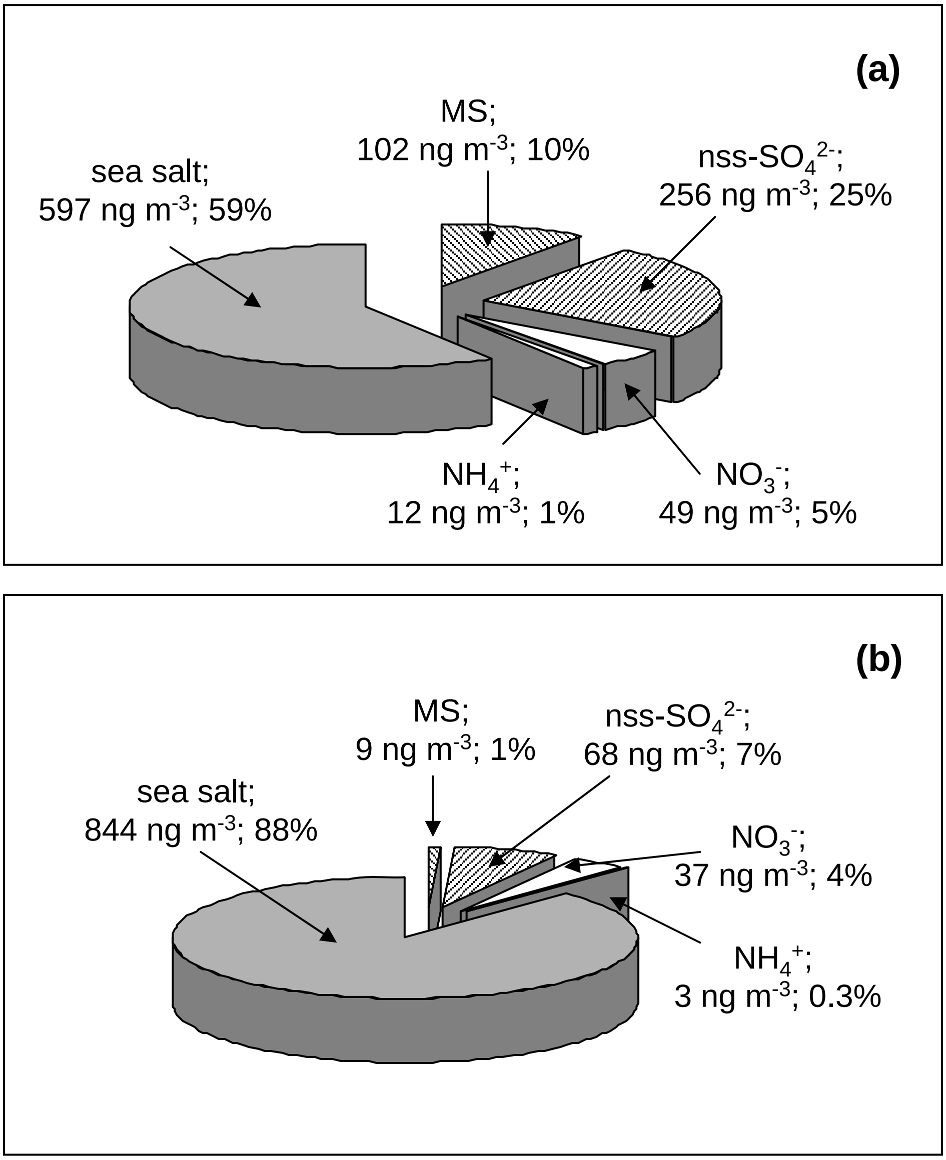


**Figure 3:** Mean ionic composition of the aerosol at Neumayer for (a) summer and (b) winter during the total measuring period (Jan. 2004 through Dec. 2006).

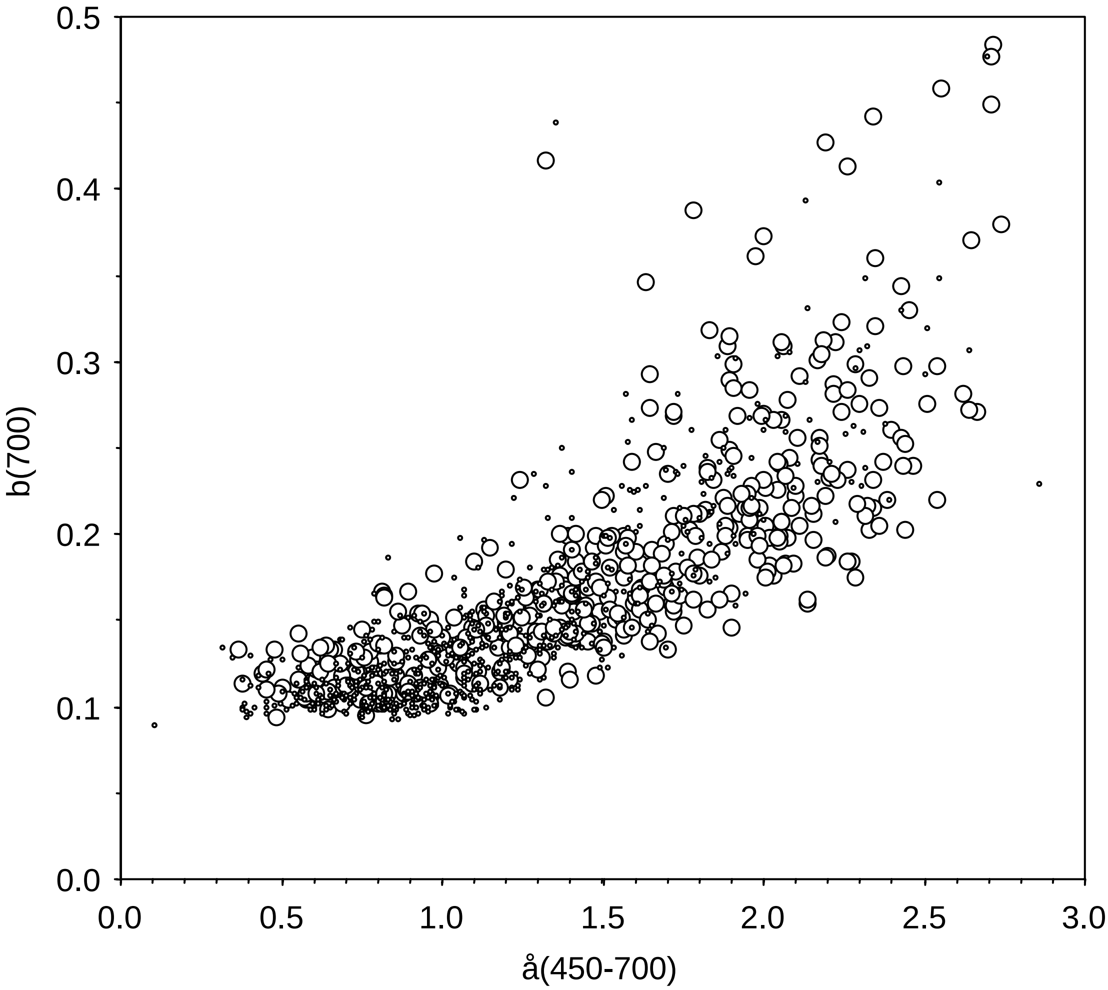


**Figure 4:** Hemispheric back scattering ratios b(700) versus scattering Ångström exponent å(450-700) for the total measuring period (Jan. 2004 through Dec. 2006); circles: summer data, dots: winter data.

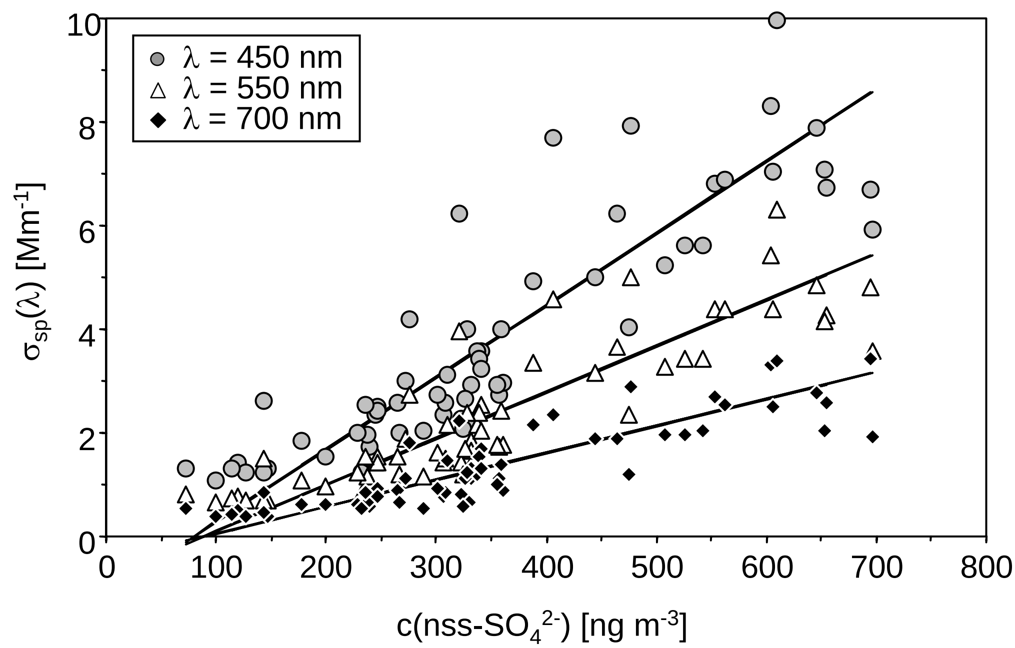


**Figure 5:** Dependence of scattering coefficients $\sigma_{sp}(\lambda)$ on nss-$SO_4^{2-}$ concentrations during days with c(nss-$SO_4^{2-}$+MS)/c(ions) >0.75. The lines represent RMA fits to the measuring points (see Table 3).

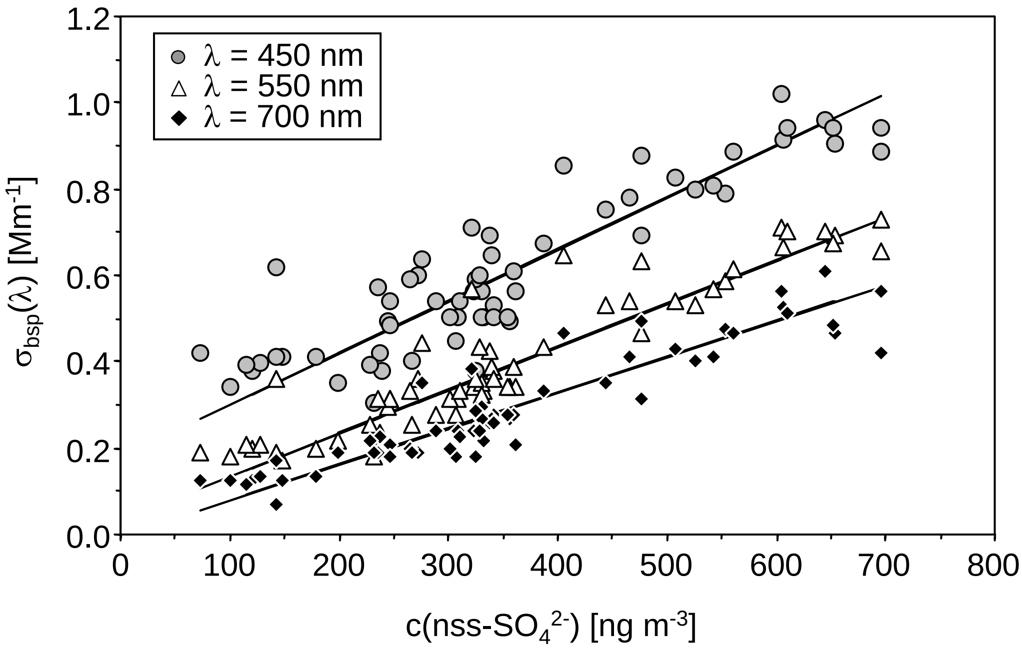


**Figure 6:** Dependence of backscattering coefficients $\sigma_{bsp}(\lambda)$ on nss-$SO_4^{2-}$ concentrations during days with c(nss-$SO_4^{2-}$+MS)/c(ions) >0.75. The lines represent RMA regression fits to the measuring points (see Table 4).

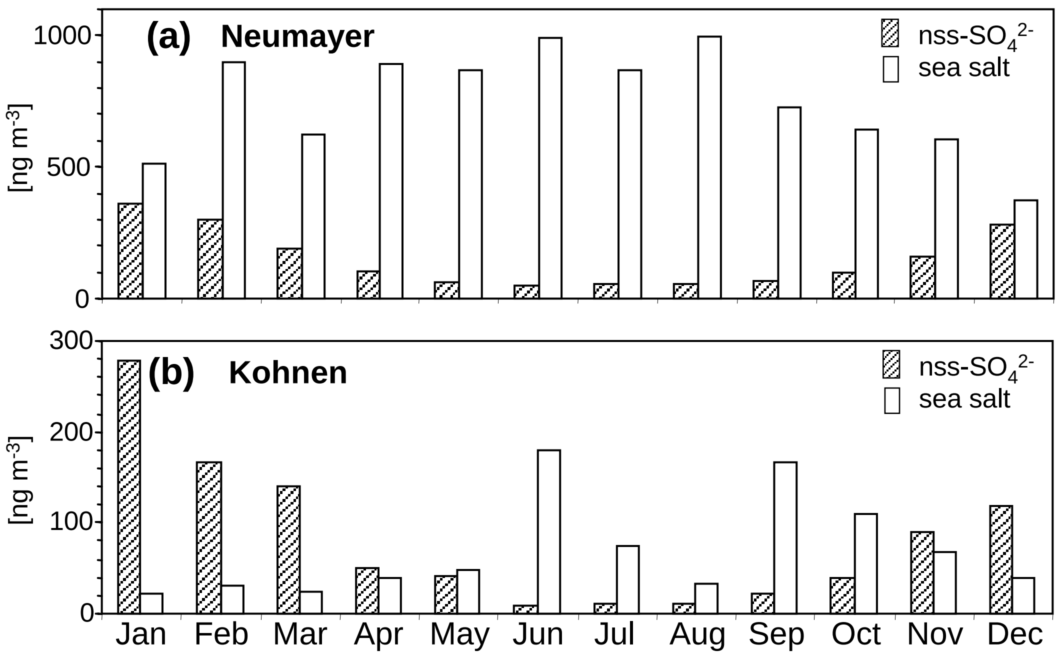


**Figure 7:** Monthly mean values of nss-$SO_4^{2-}$ and sea salt concentrations measured (a) at Neumayer. and (b) at Kohnen. All monthly mean values from Neumayer comprise measurements between January 2004 and December 2006. while the Kohnen data were obtained between January 2003 and December 2005 [*Weller and Wagenbach.* 2007].